PHYSICAL REVIEW VOLUME 68, NUMBERS 9 AND 10 NOVEMBER 1 AND 15, 1945

Shock Wave Pressures in Water Produced by Impact of Small Spheres*

J. HOWARD MCMILLEN**
Department of Biology, Princeton University, Princeton, New Jersey
(Received September 19, 1945)

Microsecond spark shadowgrams were made showing shock waves in water. The waves were produced by spheres $\frac{1}{8}''$ to $\frac{1}{4}''$ in diameter when they struck a water surface with velocities between 2000 and 4800 ft./sec. Pressures in the wave were calculated from measurements of the absence-of-light band. The pressure was found to be greatest at a point directly ahead of the sphere and to fall off to normal pressures near the surface. The waves of large pressures were observed to travel faster than a sound wave and to have velocities in accordance with the measured pressure. Because of the varying strength over the wave front, the waves have the shape of a semi-ellipse. When the entrance velocity V and projection area of the sphere were varied it was found that the pressure varied as $V^{2.17}$. It also increased linearly with the projection area of the sphere. The pressures were shown to be in fair agreement with those calculated from the compression of the water at the sphere's entrance; in the calculation an arbitrary loss of water in the splash was assumed.

WHEN an object moving with high velocity strikes the surface of water, a disturbance is produced which spreads through the water along radial lines with the point of impact as origin. The disturbance consists of a region of increased pressure and density together with a small forward motion of the medium. If the energy in the disturbance is small, the disturbance is propagated as a sound wave, but if it is large, the disturbance travels as a surface of discontinuity and is called a shock wave. While a large number of investigations[1–3] have been carried out on the propagation of shock waves in air, there has been very little reported concerning their formation and transmission through water, especially when the waves have been produced by impact. It was an interest in the relationship between the strength of the shock wave and their method of production which prompted this investigation. The experiment was directed toward determining how the pressure in the wave depended on the shape and kinematical characteristics of the impacting object.

Small spheres were used as the impacting objects because of their radial symmetry. These were shot into the water with high velocities so as to produce waves of strength sufficient to give the shock wave characteristics. The velocity range extended from about 2000 ft./sec. up to the velocity of sound in water 4800 ft./sec. Since the sphere travels with a subsonic velocity and since it is considerably retarded, the wave detaches itself from the sphere soon after it is produced. Thus this investigation has been one of detached waves.

The spark shadowgraph method was used to study these waves. It has been widely used to study shock waves in air[4, 5] ever since its development by Boys[6] in 1893. The method has the advantage of showing the general disposition of the wave at one observation. It is also well suited for measuring the pressure at the front of the wave where the pressure rises abruptly.

APPARATUS AND METHOD

The spark shadowgraphs were produced by light from a point-source spark of short duration. The light traversed a small tank with Plexiglas walls a few microseconds after the missile had struck the surface; the shadow of the shock wave was recorded on a photographic plate

* This work has been carried out under a contract recommended by the Committee on Medical Research between the Office of Scientific Research and Development and Princeton University.
** On leave of absence from Kansas State College, Manhattan, Kansas.
[1] G. I. Taylor and J. W. Maccoll, W. F. Durand's *Aerodynamic Theory* (Verlagsbuchhandlung Julius Springer, Berlin, 1935), Vol. III
[2] A. Busemann, *Handbuch der Experimental Physik*, Vol. 4.
[3] J. Ackeret, *Handbuch der Physik* (Verlagsbuchhandlung Julius Springer, Berlin, 1927), Vol. 7.
[4] D. C. Miller, *Sound Waves Their Shape and Speed* (The Macmillan Company, New York, 1937).
[5] C. Cranz and K. Becker, *Lehrbuch der Ballistik* (Verlagsbuchhandlung Julius Springer, Berlin, 1926), Vol. III.
[6] V. Boys, Nature **47**, 415 (1893).

which was placed just beyond the tank. The experimental arrangement is shown in Fig. 1(a), with the spark S, the tank T, the photograph plate PP, and the missile path G.

The spark was mounted in a brass tube two inches in diameter with a window having an area of 0.006 cm^2. The electrodes were cut from magnesium rod. A detailed drawing of the spark is shown in Fig. 1(b). The potential across the spark was 4400 volts. The flash discharged four oil-impregnated filter condensers which were connected in parallel giving a capacitance of 0.20 microfarad. Since a discharge of long duration blurs the shock-wave image, the spark was constructed with low resistance leads. Condensers with low resistance supports and plates were also chosen. The arrangement of several condensers in parallel was found to be best as this reduced the total condenser-plate resistance. Since a low capacitance produces a short discharge, the capacitance was kept as low as possible but still sufficiently high to form the desired image on the photographic plate. The duration of the spark was tested by making spark shadowgraphs of spheres traveling in air with a velocity of about 5000 ft./sec.; at this velocity the sphere travels 1.5 mm per microsecond. From the photographs it was estimated that the effective spark-duration did not exceed a tenth of a microsecond.

A wire grid, labeled Q in the figure, triggered the spark when the missile broke one of its wires. The grid was made of No. 32 copper wire spaced about 2 mm apart. Breaking the wire grid operated a thyratron-controlled spark coil which produced a discharge between the trigger electrode and the body electrode in the main spark.

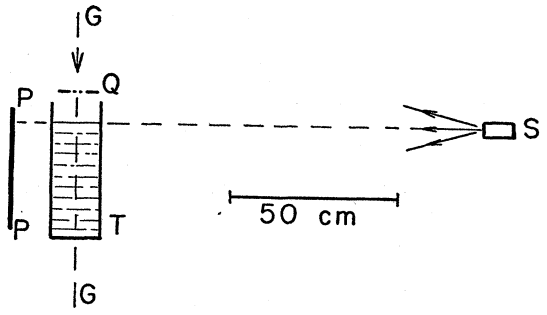

FIG. 1(a). Diagram of apparatus.

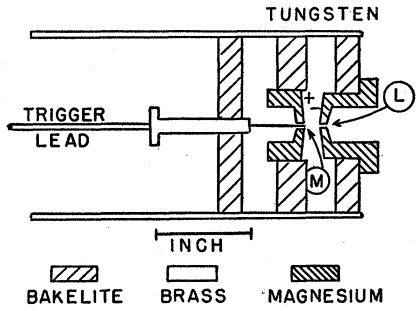

FIG. 1(b). Detail diagram of spark. Light emerges from hole L (drilled with No. 65 drill) after spark is triggered by third electrode in hole M (No. 43 drill).

An adjustable capacitance delay was also incorporated in the circuit.

The tank had two supporting walls of $1\frac{5}{8}''$ wood and two transparent walls of $\frac{1}{4}''$ Plexiglas. The distance between the wood walls was $14\frac{1}{2}''$ and between the Plexiglas $5\frac{1}{2}''$; the water was $10\frac{1}{2}''$ deep.

The spark shadowgraph was recorded on a 11×14-inch photographic plate which was placed 17.2 cm from the path of the missile. The path of the missile was also in the center of the tank. Eastman Kodak lantern slide plates of medium contrast were used. They were developed in D-72 (one:one) for five minutes.

The spark, 120 cm from the path of the missile, was placed on a line parallel to the water surface and perpendicular to the face of the tank and photographic plate. In order to convert measurements that were made on the plate to corresponding distances at the missile path, a spark shadowgraph picture was made of transparent rulers held in the path of the missile. The shadowgraph was found to have a magnification of 1.11 diameters.

Light rays which deviate from a point along the path of the missile have their deviation angle altered as the rays pass from the water to the air. For small angles near normal incidence, the distance separating two rays incident on the photographic plate was calculated to be 18.2 percent larger than it would have been if no refraction took place. This latter correction was applied to the measurements of the shock wave band widths.

Small steel balls having diameters from $\frac{2}{32}$ to $\frac{8}{32}$ inches were used as missiles. Their diameter

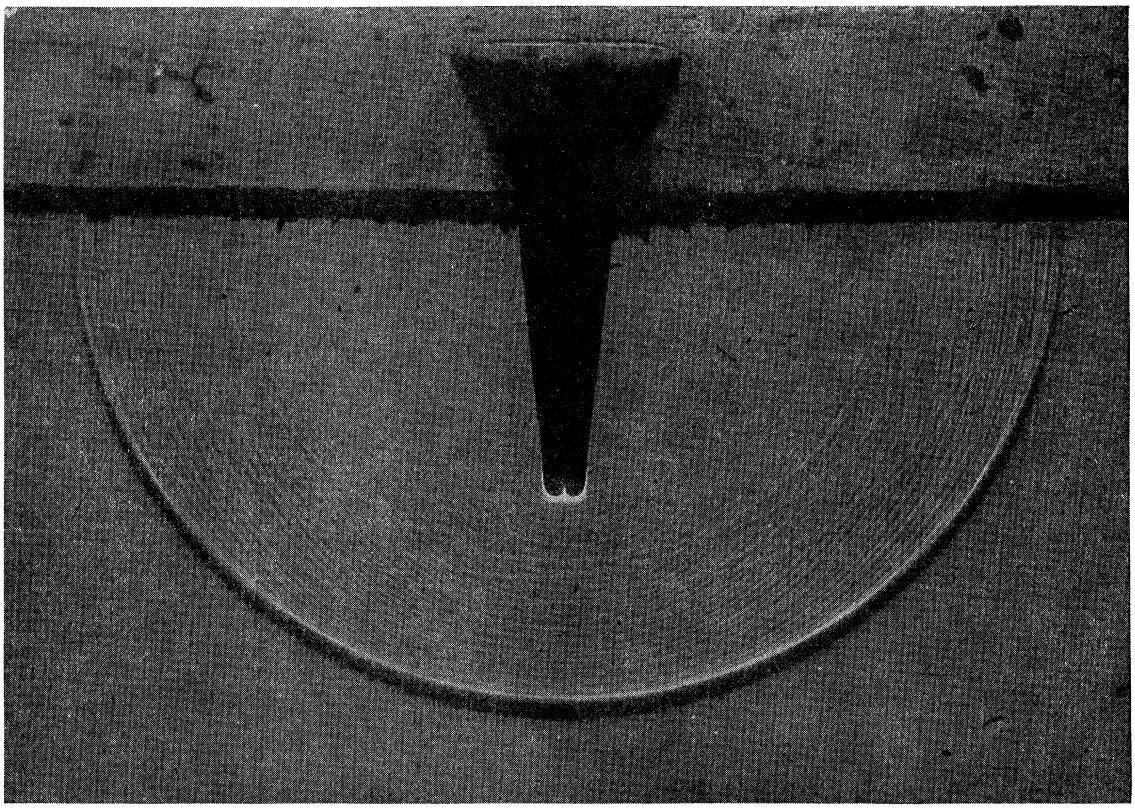

FIG. 2. Spark shadowgram of a wave after advancing 7.8 cm into the water. It was formed by a 4/32" steel sphere having an impact velocity of 3520 ft./sec.

variation as well as sphericity variation was 0.000025 inch; their density was 7.78. These were held in a cylindrical sabot about 16 mm long, split in half longitudinally, and lathe-turned to fit the caliber 30 army standard primed shell. The sabot was made of dowel-pin wood for velocities less than 4000 ft./sec., but for velocities greater than this a "Textalite" plastic sabot was used. The missile was shot from a 30 caliber Winchester smooth-bore test-action rifle. When the missile emerges from the gun, air resistance separates the two halves of the sabot which are stopped by a board with a hole in the center through which the sphere passes. There was nothing about the apparatus that would give the sphere a definite spin, but it was not impossible for the sphere to pick up some rotary motion in its flight. The velocity of each shot was measured just before the sphere hit the surface. The velocity measuring apparatus had an accuracy of about one percent.

DESCRIPTION OF CAVITY AND WAVE

The spark was set off with any time delay up to 20 microseconds after the sphere had struck the surface, catching the wave somewhere between the surface and a point 28 cm below. Since the spheres had subsonic velocities and since they were retarded upon hitting the water, the sphere with its conical cavity lagged behind the wave. Figure 2 shows a wave that has penetrated 7.8 cm. The sphere velocity was 3,520 ft./sec., and it had lost 35 percent of its velocity at the time the shadowgram was taken. The shock wave has a presence-of-light band and an absence-of-light band, the latter being much wider than the one generally observed in air. Its center, as far as can be determined, is at the surface of the water.

The air-filled cavity behind the sphere is opaque to light and casts a sharp silhouette. At the tip of the cavity light is so concentrated

as to form an illuminated cusp. As the sphere slows down, the cusp gradually disappears, and at low velocities became a mere speck of light. The shadow of the ball is not visible in the cavity, but its position can be located by using x-ray shadowgrams. These were taken with a Westinghouse Micronex Surge Generator[7] which produces an x-ray flash of less than a microsecond duration. The flash was produced by discharging a 0.0066-μf condenser at 180,000 volts through a cold-emission x-ray tube. The water tank consisted of a cardboard box containing about 200 cm^3 of water. The true shape of the cavity was also determined since x-rays, unlike rays from the spark, do not refract. Figure 3 shows these two kinds of shadowgrams when a $\frac{6}{32}''$ sphere is shot into water with a velocity of about 2,700 ft./sec. The sphere has penetrated about 3.5 cm in both shadowgrams. By comparing the two pictures one can show that the center of the sphere is at the tip of the cusp. Thus the cusp is formed by light bent around and behind the sphere.

The spark shadow of the cavity in the vicinity of the sphere is wider than the geometrical shadow. In Fig. 3 the width at the level of the center of the sphere is 38 percent wider than the true width as shown in the x-ray. This anomalous width is present for a distance of several sphere diameters up the cavity but in decreasing magnitude. At higher sphere velocities the increase in width is greater; a doubling of the width has been frequently observed.

The concentration of light behind can be explained by the increase in pressure and density around the sphere. The pressure at the nose of the sphere reaches thousands of atmospheres which is sufficient to produce a considerable change in the refractive index. While at present the details of the manner in which these optical effects are produced are not clear, it is hoped that further study will develop a method for determining the pressure distribution around the sphere from measurements made on the cusp and the anomalous width. It is obvious from the refraction effects involved that the analysis must be one that deals with a compressible fluid.

[7] L. F. Ehrke and C. M. Slack, Elec. Eng. **54**, 149 (1935).

WIDTH OF BAND AND PRESSURE

The width of the dark band varies with the pressure in the wave. Hilton[8] has shown that for air the width is bounded by a ray tangent to the wave front and by a ray which suffers a minimum deviation in traversing the medium immediately behind the front. When this is applied to water, the fractional change in refractive index ϵ is given by

$$\epsilon = 0.272 d^{\frac{3}{2}} R^{-\frac{1}{2}} D^{-1}, \qquad (1)$$

where d is the band width, R the radius of curvature of the wave front (as measured in the photograph), and D is the distance from the point of tangency to the photograph.

In deriving Eq. (1) it was assumed that the pressure in the wave was constant over the region immediately behind the wave front. Preliminary measurements with tourmaline crystals have shown that air pressures are not constant but rather rise to a peak and then fall off with what appears to be an exponential decay. The crystal measurements are not precise enough to determine if the peak is sufficiently dull to permit the unqualified use of Eq. (1). However, in this investigation only relative changes in shock wave strength are of interest. Hence an effective $\bar{\epsilon}$ will be calculated which may be considered to be a measure of the peak value for ϵ. In the same manner $\bar{p}$ will be the effective pressure behind the wave.

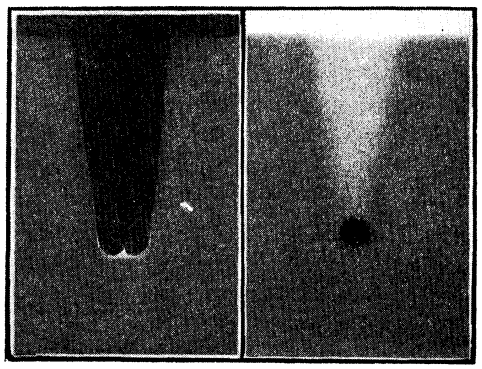

FIG. 3. Comparison of spark shadowgram and an x-ray shadowgram showing the effect of refraction in the spark shadowgram. Spheres of diameter 6/32″ and impact velocity of about 2700 ft./sec. were used.

[8] W. F. Hilton, Proc. Roy. Soc. **A169**, 174 (1938).

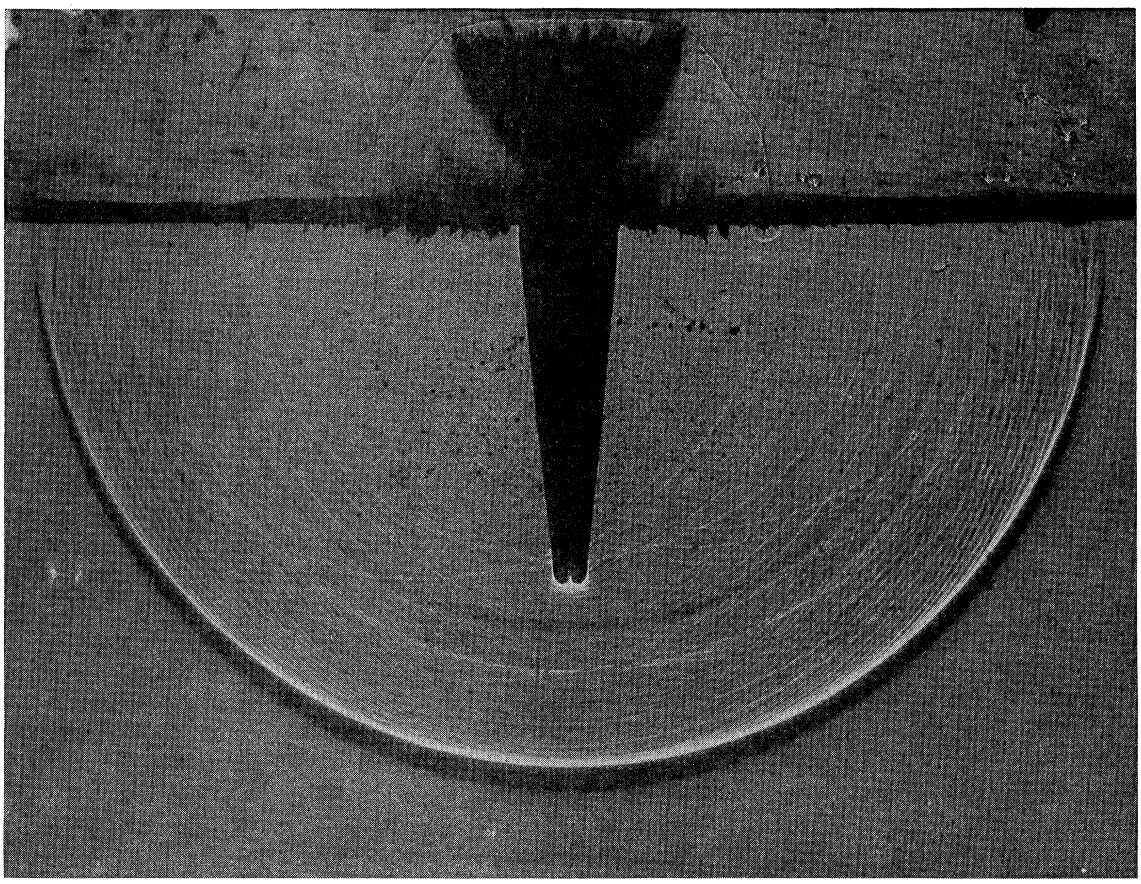

FIG. 4. Spark shadowgram showing variation in band width over shock wave front. Sphere had initial velocity of 4840 ft./sec. and a diameter of 4/32". Shock wave has penetrated 10.7 cm of water.

The next consideration is that of converting the data for ϵ into pressures. Poindexter and Rosen[9] have made a direct determination of this relationship by varying the pressure in a water-filled vessel of optical-prism shape and observing the change in deviation of a spectrum line. For low pressures such as encountered in this experiment they find $\epsilon=1.06\times10^{-5}p$ where p is in kg/cm². The only disadvantage in using this expression is that it conforms to an isothermal change, whereas the change produced by a shock wave is more nearly adiabatic.

A second approach to finding the proper relationship between ϵ and p is that of using density data. For this purpose the Rankine[10]-Hugoniot[11] expression for adiabatic changes across a shock wave can be used. At low pressures and for an adiabatic coefficient $\gamma=7.15$. This gives $\Delta\rho/\rho=4.54\times10^{-5}p$. Also Lyons[12] has shown that Newton's law relating density and

TABLE I. Showing how various theoretical laws and experimental observations give values to k_3 in the relationship $\epsilon=k_3p$. Here $k_3=k_1k_2$, $\epsilon=k_1\Delta\rho/\rho$ and $\Delta\rho/\rho=k_2p$. The pressure p is in kg/cm².

	Bridgman ($k_2=5.06\times10^{-5}$)	Rankine-Hugoniot ($k_2=4.54\times10^{-5}$)
Newton ($k_1=0.219$)	1.11×10^{-5}	0.995×10^{-5}
Lorentz-Lorentz ($k_1=0.276$)	1.40×10^{-5}	1.26×10^{-5}
Poindexter-Lyon	$.610\times10^{-5}$	

[9] F. E. Poindexter and J. S. Rosen, Phys. Rev. **45**, 760 (1943).

[10] Rankine, Phil. Trans. Roy. Soc. **160**, 277 (1870).

[11] H. Hugoniot, Journal de l'École Polytechnique, Paris Cahiers, 57–59 (1887–1889).

[12] W. J. Lyons, J. Opt. Soc. Am. **26**, 144 (1935).

refractive index changes is obeyed for water. It is $\epsilon=0.219\Delta\rho/\rho$. Thus by using Newton's law and the Rankine-Hugoniot adiabatic one obtains $\epsilon=0.995\times10^{-5}p$ which is not significantly different from Poindexter and Rosen's observation.

Two other sources of information in this field are also of interest. One is the static pressure-density determinations of Bridgman,[13] and the other is the Lorentz-Lorentz law relating ϵ and $\Delta\rho/\rho$. These have been put into Table I along with those already discussed. The table is self-explanatory; there is surprisingly little difference in the value of the constants involved when one considers the difference in the methods concerned. In this report 1×10^{-5} was chosen for the constant, it being the average of Poindexter-Rosen determination and the constant calculated from the Newton and Rankine-Hugoniot equations.

DISTRIBUTION OF SHOCK WAVE STRENGTH OVER WAVE FRONT

Because the width of the dark band is related to the strength of the wave, widths were measured under various experimental conditions. It is observed first of all that the width or strength of the wave is not the same over the wave front but is greatest directly ahead of the sphere, and least where the wave touches the surface. In addition to this general observation it is noted that the wave front changes in character at a point which is located about 7° from the surface. This is clearly shown in Fig. 4 where the black band is observed to taper off in width while approaching a point 7° along the arc. Other photographs have shown an abrupt change in the curvature of the wave front at this point, the wave below 7° being nearly parallel and perpendicular to the surface. This abrupt change in the strength of the wave at 7° is probably due to the fact that it is along this radial line that the sphere loses contact with the water during its flight. Measurements of the angle between the equatorial plane and the radial line to the point at which the water leaves the sphere gave a value of 9° 20′ with a probable error of 8′. These measurements were made on $\frac{6}{32}''$ steel spheres by means of x-ray shadowgrams. The spheres had striking velocities of about 3,000 ft./sec. and were measured at penetrations less than 5 cm.

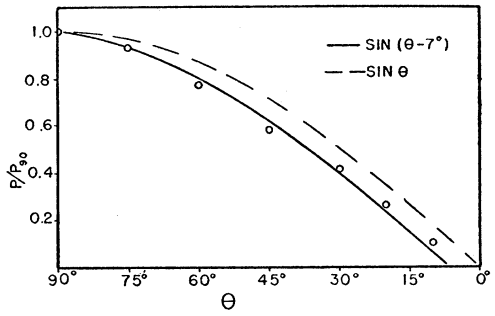

FIG. 5. Showing the angular distribution of pressure over the wave front relative to that straight ahead at $\theta=90°$.

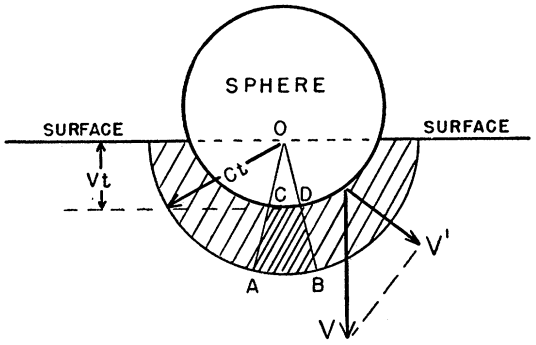

FIG. 6. Schematic sketch showing compressed water volume as sphere enters the water, the compressed volume being trapped between the shock wave front and the sphere.

The width of the dark band was measured for eight different shots, and the average value recorded. To facilitate comparisons all measurements were adjusted for unit width at the 90° position. The sphere velocities varied from 1800 to 4840 ft./sec. and both $\frac{4}{32}''$ and $\frac{6}{32}''$ spheres were used. Since the effective pressure $\bar{p}$ is proportional to $d^{\frac{3}{2}}$ an empirical relationship between $d^{\frac{3}{2}}$ and θ was sought. While it was observed that at angles less than 75° the rate at which the pressure changed with angle was nearly constant, the following expression gave a better agreement at all angles

$$\bar{p}=\bar{p}_{90}\sin(\theta-7). \qquad (2)$$

Here θ is the angle in degrees and $\bar{p}_{90}$ is the pressure directly ahead of the sphere, at $\theta=90°$. The curve for the above expression and the experimental data are shown in Fig. 5.

[13] P. W. Bridgman, Proc. Am. Acad. Sci. **12**, 347 (1911).

This falling off in pressure along the shock wave front, as radial lines which are more nearly parallel to the water surface are considered, can be partly understood by making use of Fig. 6 where a drawing of a sphere just entering the water is shown. The arc described by the radius Ct represents the shock wave front. The pressure imparted to the medium is proportional to the velocity of the moving sphere normal to the wave front which in the diagram is represented

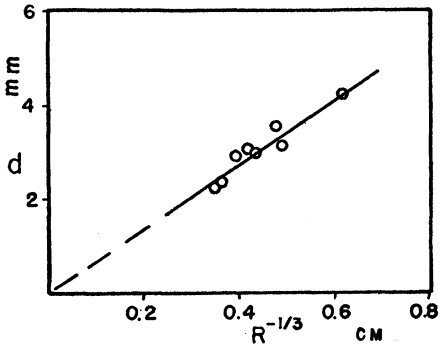

FIG. 7. Showing that the band width is a linear function of $R^{-\frac{1}{3}}$, or that the pressure falls off as R^{-1}. Steel spheres 4/32" in diameter traveling with a velocity of 3600 ft./sec. were used.

by the vector **V'**. When the sphere enters the water with a velocity close to the velocity of the shock wave, the velocity vector **V'** is nearly normal to both the wave front and the sphere. Since the above measurements were made on spheres having nearly sonic velocities, one can assume that the velocity and pressure along a radial line designated by θ is approximately proportional to $V \sin\theta$ or simply $\sin\theta$. The curve for $\sin\theta$ is also plotted in Fig. 5, and it is seen that while it has the general shape of the experimental curve its values for the pressures are larger than those found in the experiment.

One of the surprising observations on the angular distribution of the width of the shock wave band comes with the discovery that the distribution changed very little when missiles of quite different shapes were used. Small cylinders striking edge-wise and cones with apex angles equal to 90° produced waves which by inspection resemble those produced by the spheres. This was also true for pieces of wood of irregular shape which occasionally strike the water. Evidently the transfer of momentum to the water cannot be explained entirely in terms of velocity components normal to the missile's surface, as it was above for the sphere.

DECREASE IN SHOCK WAVE STRENGTH WITH DISTANCE

The spark shadowgrams of waves having the same strength show that those that have advanced further into the tank are weakest. This is understandable since the energy per unit volume decreases with the geometrical expansion of the wave front. The energy per unit volume E decreases as R^{-2}. If one neglects changes in the entropy as the wave front expands, then $E=\int pdv$, and at low pressures $dv=-kdp$. It follows that

$$E=(1/2)kp^2-(1/2)kp_0^2.$$

Neglecting the second term and remembering that E is proportional to R^{-2}, one obtains

$$p=k'R^{-1};$$
$$d=k''R^{-\frac{1}{3}}.$$

Thus while the pressure falls off fast with increasing R, the width decreases relatively little. This difference arises from the fact that an increase in radius of the spherical wave front also increases the deviation of the minimum ray.

To test this pressure-distance relationship, band widths were measured at penetration depths ranging from 4.25 to 21.95 cm. To obtain the photographs of penetrations near 20 cm, the spark was lowered below its original water level position so that the corrections on D and d, due to the geometry of the apparatus, became negligible. Since the spheres did not all have the same velocity, the band width was reduced to correspond to a band width at a velocity of 3600 ft./sec.; experimental data described in a succeeding section was used for this. The test was carried out with a $\frac{4}{32}$" steel sphere, and the band width was measured at the 90° position on the arc. The results are shown in Fig. 7 where d is plotted against $R^{-\frac{1}{3}}$. The linearity of the plotted points shows that the effective pressure in the shock wave falls off according to R^{-1}. Unfortunately the width is such a slowly varying function of R that small deviations from the R^{-1} law would not be observed in this experiment. It is not possible, for example, to observe the effect

of changes in the entropy which may accompany the expanding wave.

VARIATION OF WAVE VELOCITY WITH PRESSURE

When the high pressure shock waves are examined it is seen that the wave front does not describe a perfect arc of a circle but is elongated in the direction of the missile's flight, forming an ellipse of small eccentricity. The wave front in line with the sphere's trajectory is stronger and travels with greater speed while the wave near the surface travels with sonic velocity. The eccentricity is so small that it can only be measured for spheres traveling with velocities around 4000 ft./sec. or larger.

Measurements on four plates gave percentage differences $\Delta R/R$ between the long and short axis of the elliptical wave front ranging from 1.9 to 4.3 percent. This is interpreted as meaning that the average wave velocity in the strong portion of the front was from 1.9 to 4.3 percent faster than the velocity of sound in water. These data are collected in Table II. In the fourth column the average Mach number which the wave possesses during its flight is recorded; the Mach number is the ratio of wave to sound velocity, and it is continually decreasing as the wave expands and weakens.

That shock wave velocity depends on its strength is well known.[1] If the velocity of a plane shock wave is C and the velocity of the medium is u, then the conservation of mass across the wave front requires that

$$\rho_0 C=\rho(C-u). \tag{3}$$

The momentum imparted to the water equals the pressure difference so that

$$p-p_0=\rho_0 Cu. \tag{4}$$

Eliminating u from the above gives for the velocity of the wave

$$C^2=\rho(p-p_0)/((\rho-\rho_0)\rho_0). \tag{5}$$

When the conservation of energy is taken into account and Tammann's[14] equation of state,

$$(p+3000)v=KT,$$

is used, a relationship between p, p_0, ρ and ρ_0 is found; this is the well-known Rankine[10]-Hugoniot[11] equation

$$\frac{\rho_0}{\rho}=\frac{(\gamma+1)P+(\gamma-1)}{(\gamma-1)P+(\gamma+1)}, \tag{6}$$

where $\gamma=7.15$ and is the adiabatic constant, and $P=(3001)/(p+3000)$. The pressure p is in atmospheres.

By making use of (6) and (5), pressures corresponding to the Mach numbers observed above were calculated. These are recorded in Table II along with pressures calculated from the band width at the forward portion of the wave. It is observed that the average pressure in the wave during flight as measured from the ellipticity of the wave front is larger than that calculated from the band width. This is as it should be, since the band width measurement gives the final pressure only. While it would be interesting to calculate the final pressure in terms of the average pressure and thus correlate it with the pressure obtained from band widths, two factors make it inadvisable. One of these is the experimental difficulty entailed in measuring the eccentricity of the elliptical wave front; the other is the difficulty in knowing how the pressure varies with R at the limit, when R is zero or comparable with the sphere diameter.

TABLE II. Average Mach numbers for several wave fronts as determined from the eccentricity of the wave. Also a comparison of pressure in wave measured from band width and from average Mach number.

V ft./sec.	R cm	$\Delta R/R$	Average Mach number	Pressure kg/cm² From Mach number	From width of band
4,730	9.8	0.043	1.043	462	137
4,840	11.8	0.034	1.034	371	141
4,480	12.13	0.031	1.031	337	102
4,090	9.45	0.019	1.019	205	95

VARIATION OF SHOCK WAVE PRESSURE WITH IMPACT VELOCITY

Inspection of the shadowgrams shows that the band width becomes larger as the impact velocity of the sphere is increased. The difference in width can be seen in Fig. 8 where a shadowgram for a $\frac{4}{32}$" sphere having a velocity of 1830 ft./sec. is shown; this may be contrasted with Fig. 4,

[14] G. Tammann, Ann. d. Physik **37**, 975 (1912).

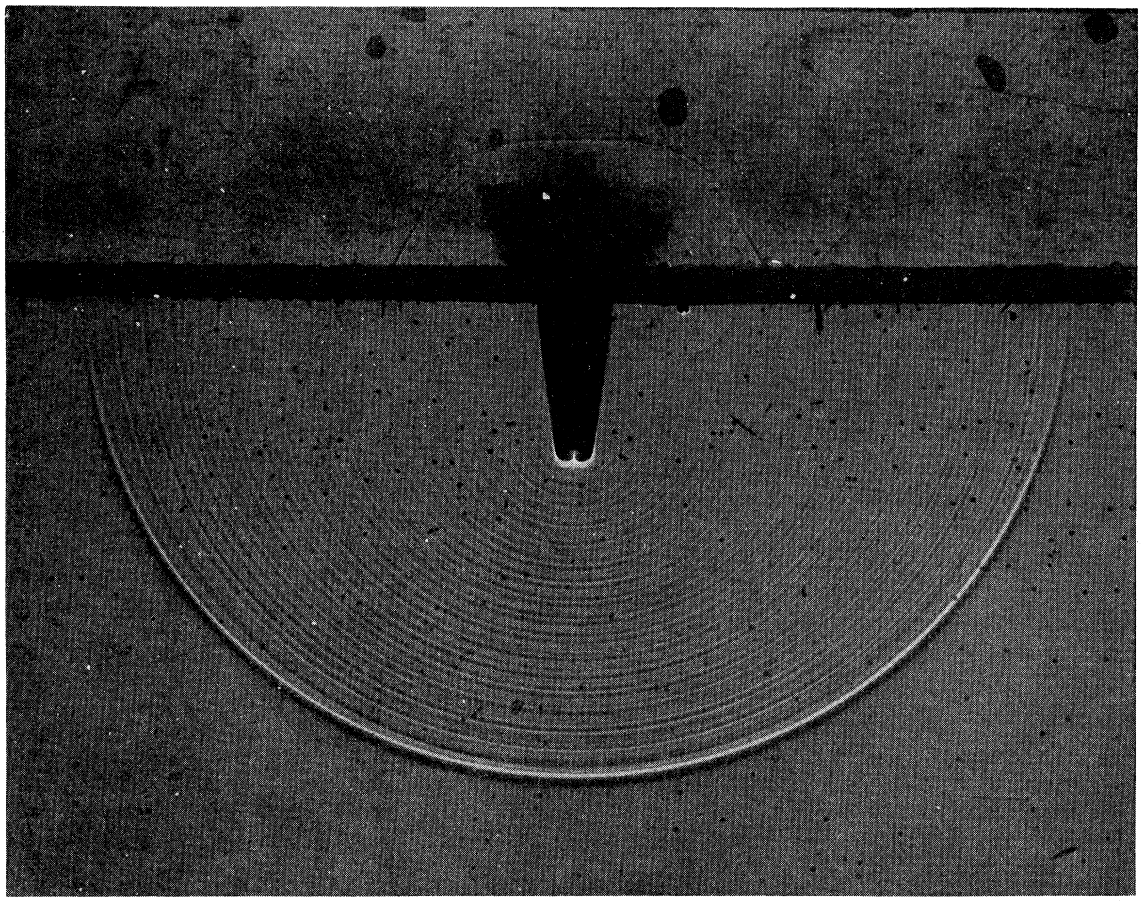

FIG. 8. Spark shadowgram of shock wave produced by a low velocity sphere. The 4/32″ steel sphere had an initial velocity of 1830 ft./sec. Shock wave has penetrated 6.5 cm of water.

showing a wave formed by the same sized sphere traveling with a velocity of 4840 ft./sec. A series of seventeen shots were made at different velocities to determine just what relationship does exist between pressure and impact velocity. The $\frac{4}{32}''$ steel spheres were used, and the velocities ranged from 1830 to 4840 ft./sec.; the latter is just above the velocity of sound in water. All measurements were made at $\theta=90°$, that is, at the foremost point of the wave.

The spark was triggered so that the wave was shadowgraphed as close to a 10-cm penetration as possible; all measured waves fell between 7.0 and 15.2 cm. The width was measured with a vernier caliper with an accuracy which was estimated to be ± 0.01 cm. All widths were reduced to correspond to a wave penetration of 10 cm by making use of the already established fact that the width varies as $R^{-\frac{1}{3}}$. The widths were further reduced to correspond to $D=17.2$ cm for those shots which did not follow the aim of the gun. The spheres rarely strayed more than a centimeter from the central position. Still another correction consisted of one for the refraction of the diverging rays as they passed from the water to the air. The data are plotted in Fig. 9.

By making use of Eq. (1) these widths were employed to calculate the effective index change $\bar{\epsilon}$ and effective pressure $\bar{p}$ at the front of the shock wave. The data are recorded in the logarithm plot of Fig. 10. The points are observed to fall on a straight line having a slope 2.17. The data conform to the empirical relationship

$$\epsilon=6.07\times 10^{-4}V^{2.17}, \tag{7}$$

where V is the impact velocity in kilometers per second. The corresponding expression for effective pressure is

$$p=607\,V^{2.17}R^{-1}, \tag{8}$$

where V is in kilometers per second, R in cm and p in kg/cm^2. It is to be remembered that the above formula applies only to a $\frac{4}{32}''$ steel sphere.

The increase in pressure with sphere velocity can be partially explained by making certain simplifying assumptions regarding the events which occur at entry. It is assumed first of all that the compressible water is trapped between the shock wave front and the sphere entering the water. It is also supposed that part of the water escapes in the splash so that the trapped volume is smaller than at first supposed.

Let the sphere be in the process of entering the water as shown in Fig. 6. The compressed region is contained between the sphere and the wave front of radius, Ct, where C is the wave velocity and t a small time interval. During this same time interval the sphere advances a distance Vt.

In the cone OAB (the pressure within which determines the pressure at the center of the wave front) the volume is reduced to $ABCD$. The new density ρ is given by

$$\frac{\rho_0}{\rho}=\frac{(Ct)^3-s(Vt)^3}{(Ct)^3}, \tag{9}$$

where ρ_0 is the original density of the water, and s represents that fraction of water volume swept out by the sphere which is not lost in the splash.

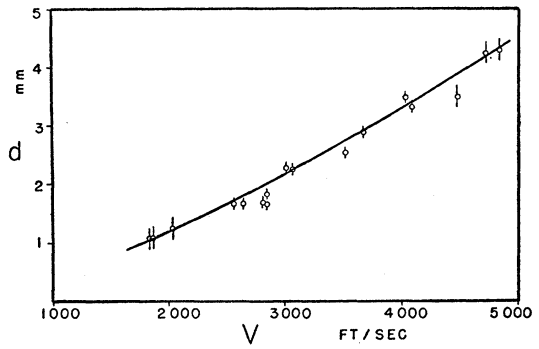

FIG. 9. Showing how band width at the forward portion of the wave varies with impact velocity; 4/32″ steel spheres. The length of vertical dashes indicates estimated error in measuring the bands. $R=10$ cm, $D=17.2$ cm.

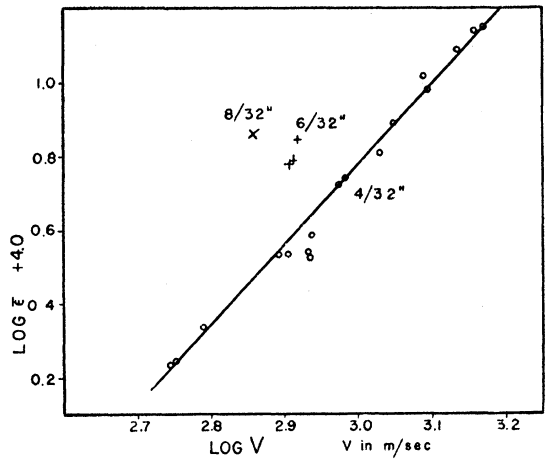

FIG. 10. Showing a logarithmic plot of effective refractive index and effective pressure as a function of sphere velocity; 4/32″ steel sphere, $\theta=90°$, $R=10$ cm.

The above reduces to

$$\rho_0/\rho=1-s(V/C)^3.$$

A fair agreement with the experimental data is obtained by setting $s=0.25$; this calls for a large loss of water when it is compared to the volume of the sphere, but in absolute magnitude it is quite small.

The pressures equivalent to the density ratios calculated from the above were obtained from the Rankine-Hugoniot Eq. (6). After the pressures were calculated for various sphere velocities they were reduced to a wave position of 10 cm. In this reduction use was made of the observation that the pressure in the wave falls off inversely as the first power of the distance. Since it was necessary to assume a value for the radial distance at which the wave was created, a distance equal to the sphere diameter was chosen.

The calculated pressure-curve and the experimental data are shown in Fig. 11. One observes that the calculated pressure increases with velocity and agrees in absolute magnitude near a velocity of 2500 ft./sec. At velocities approaching the velocity of sound in water, however, the calculated pressures deviate considerably from those observed experimentally. For a treatment of this problem at high velocities a more detailed analysis of the volume of water lost in the splash is called for.

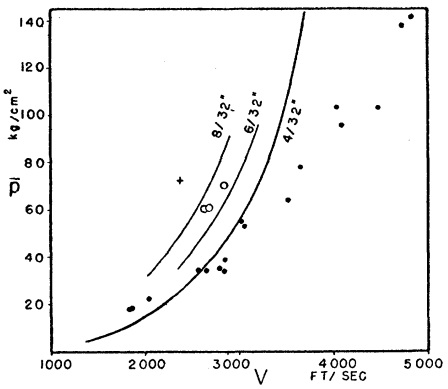

FIG. 11. Showing measured pressures (points) of wave as a function of velocity; $R=10$ cm, $\theta=90°$. The curve is the calculated pressure based on a loss of water in the splash and the Rankine-Hugoniot compression law. It was assumed that the wave originated at a point below the surface which was equal to the diameter of the sphere.

WAVE STRENGTH VARIATION WITH PROJECTION AREA AND DENSITY

Shock wave patterns from a great variety of missiles have been observed. These include small specks of wire from the trigger screen with areas less than a 0.002 cm² and pieces of wood (parts of the sabot) having areas of about 1.0 cm². It is clear from inspecting these shadowgrams that the missiles having large projection areas produce the widest bands.

To find the relationship between projection area and shock wave strength, shadowgrams were made with $\frac{4}{32}''$, $\frac{6}{32}''$, and $\frac{8}{32}''$ spheres. The width at the 90° position along the arc was then measured. This width was then corrected and reduced according to the methods described in the previous section. Log $\bar{\epsilon}$ values for the data of the $\frac{6}{32}''$ and $\frac{8}{32}''$ spheres were inserted in the graph of Fig. 10. There was only one point for the $\frac{8}{32}''$ sphere; since it was found, while acquiring this datum, that an $\frac{8}{32}''$ sphere breaks the tank.

Lines were drawn through the experimental points in Fig. 10 which were parallel to the line for the $\frac{4}{32}''$ sphere. From the intercepts the constant appearing in Eq. (8) was determined for the $\frac{6}{32}''$ and $\frac{8}{32}''$ sphere. When these are plotted against projection area of the sphere as they are in Fig. 12, a linear relationship is found. Thus the pressure in a shock wave increases linearly with the sphere's projection area A. The pressure is given by the formula

$$\bar{p}=(300+3920A)\,V^{2.17}R^{-1},$$

where R is in cm, V in kilometers/sec., A in cm and $\bar{p}$ in kg/cm².

A study was made of the effect of sphere density on the strength of the shock waves. A comparison was made of the band width and pressure when the wave was produced by aluminum and steel spheres. The aluminum spheres were 0.277 times lighter than those of steel. The velocity for all shots were kept nearly the same, the average being 2870 ft./sec.; $\frac{4}{32}''$ spheres were used throughout. It was found that the wire-screen trigger could not be used to trigger the aluminum sphere, since the wire cut the aluminum and destroyed its sphericity. A microphonic trigger was used in place of it. This consisted of a carbon microphone and amplifier which fed into the delay circuit.

The spark shadowgraphs showed no apparent difference between the bands formed by the aluminum spheres and those of steel. The data are collected in Table III where the pressures for two aluminum shots relative to those of steel are given. The density ratio is also given for comparison. The pressure that was used for the steel sphere was an average of three shots. One observes that there is no appreciable difference in the pressures even though the density change is about threefold. This lack of importance on the part of density is frequently observed in the spark shadowgraphs when fragments of the wooden-sabot accompany the sphere through the

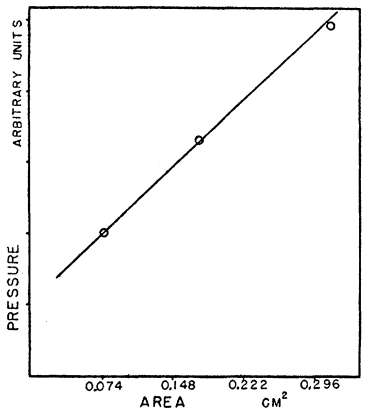

FIG. 12. Showing how the shock wave pressure increases linearly with the projection area of the sphere.

sabot catcher and also strike the water. They produce a very wide band in spite of their small density.

These observations of the effect of sphere size on the strength of the shock wave can be explained, in part, by referring to the model of the impact-action which was introduced in the previous section. In this model two arbitrary parameters were introduced; one was the coefficient representing the loss of water by splash, while the other was the distance below the surface at which the wave was considered to be formed.

One observes, first of all, that an analysis based on the model is independent of density which is in agreement with the experiment. Likewise the model calls for an increase in pressure with projection area as was also observed; however, the rate of increase is different. For the model the pressure increases as $A^{\frac{1}{2}}$ while it was observed to increase proportional to (constant$+A$). The calculated and measured pressures, as they depend on A, are plotted in Fig. 11. The calculated values are too small, showing that a more rigorous treatment than the one furnished by this simple model is needed.

TABLE III. Comparison of shock wave pressure for aluminum and steel spheres. Diameter $=4/32''$, $V=2870$ ft./sec.

Exp. no.	$\bar{p}_{Al}/\bar{p}_{Fe}$	ρ_{Al}/ρ_{Fe}
64	1.08	0.277
59	1.03	

ACKNOWLEDGMENTS

The author is pleased to acknowledge his appreciation to Dr. E. Newton Harvey for suggesting this investigation and for the many stimulating discussions which accompanied it. He also wishes to thank Mr. Harold Towne and Mr. James Hay for their help in obtaining the experimental data.

Erratum: Refraction Effects in Electron Diffraction

LORENZO STURKEY AND LUDO K. FREVEL
The Dow Chemical Company, Midland, Michigan

[Phys. Rev. **68**, 56L (1945)]

AN error was made in the equation included for δ, the deviation of diffraction angle from the Bragg angle. The correct form should be:

$$\delta=(\pm[\tan r_1]\pm[\tan r_2])(P/2E).$$

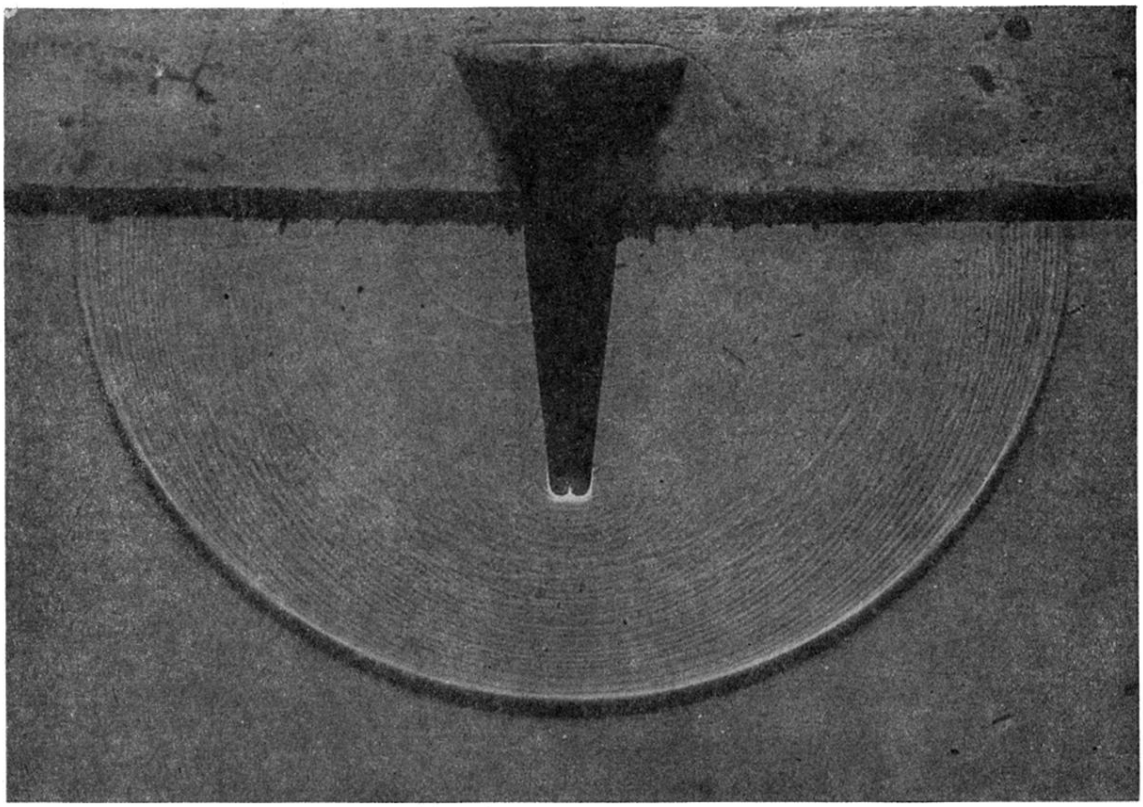

FIG. 2. Spark shadowgram of a wave after advancing 7.8 cm into the water. It was formed by a 4/32″ steel sphere having an impact velocity of 3520 ft./sec.

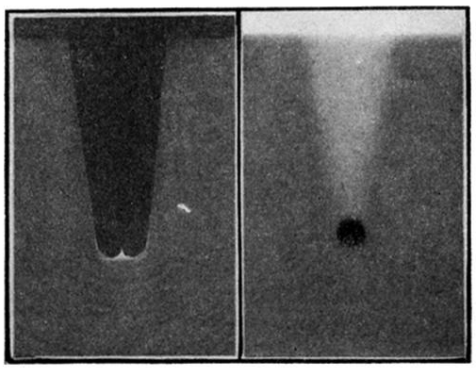

FIG. 3. Comparison of spark shadowgram and an x-ray shadowgram showing the effect of refraction in the spark shadowgram. Spheres of diameter 6/32″ and impact velocity of about 2700 ft./sec. were used.

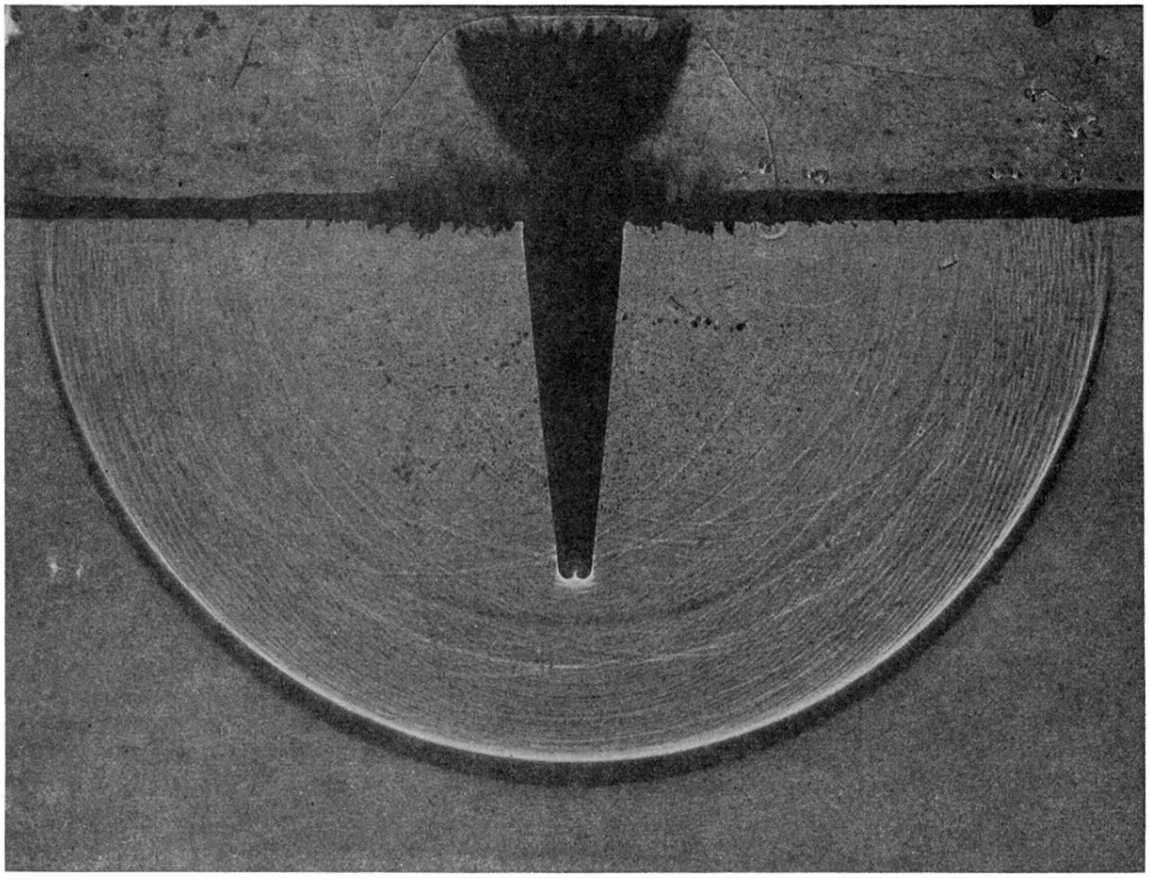

FIG. 4. Spark shadowgram showing variation in band width over shock wave front. Sphere had initial velocity of 4840 ft./sec. and a diameter of 4/32″. Shock wave has penetrated 10.7 cm of water.

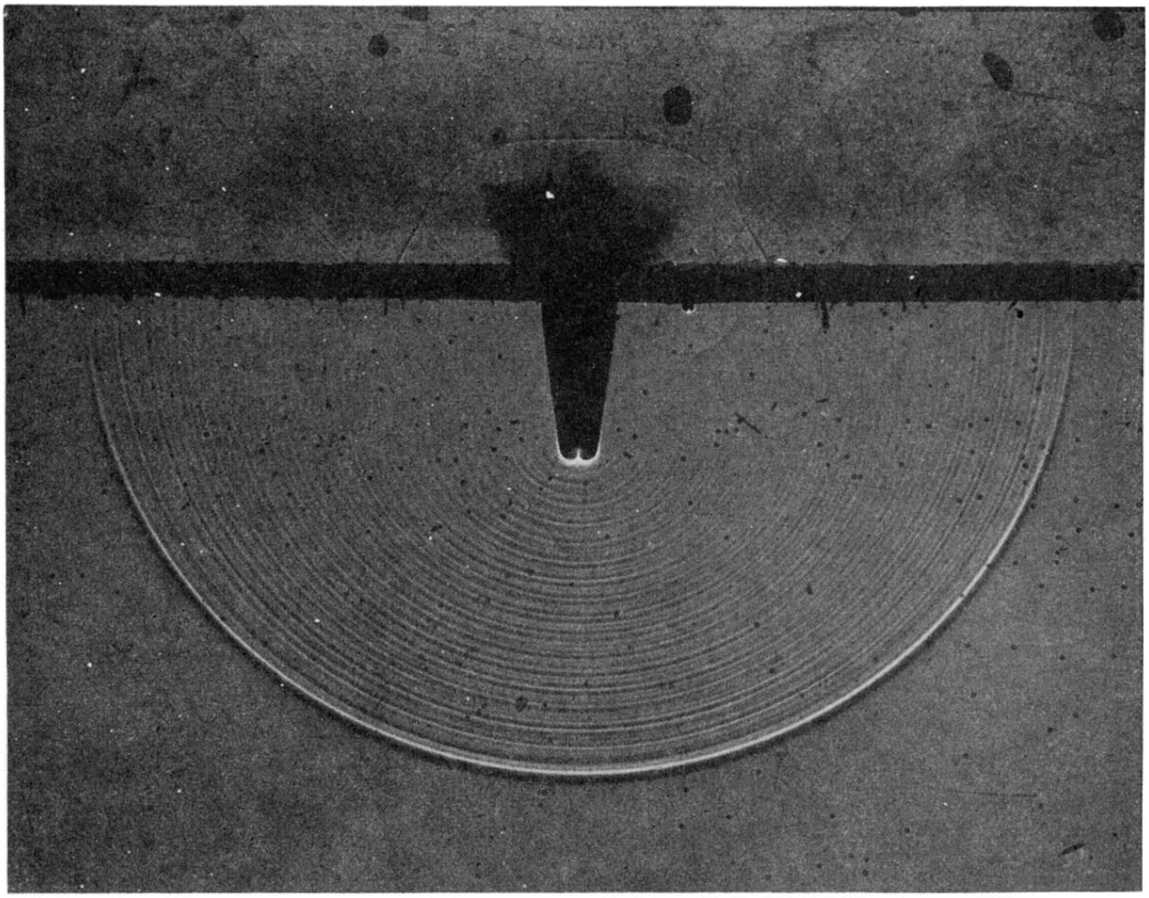

FIG. 8. Spark shadowgram of shock wave produced by a low velocity sphere. The 4/32″ steel sphere had an initial velocity of 1830 ft./sec. Shock wave has penetrated 6.5 cm of water.